Submitted to

32nd International Conference on High Energy Physics, ICHEP04, August 16, 2004, Beijing
Abstract: **6-0178**
Parallel Session **6**

www-h1.desy.de/h1/www/publications/conf/conf_list.html

Diffractive $D^{*\pm}$ Meson Production in Deep-Inelastic Scattering at HERA

H1 Collaboration

Abstract

A new measurement is presented of $D^{*\pm}$ meson production in diffractive deep-inelastic scattering at HERA. The data were collected in the years 1999 and 2000 and correspond to an integrated luminosity of 42.6 pb^{-1}. Cross sections are measured for the process $ep \to eXY$ where the system X contains at least one $D^{*\pm}$ meson and is separated by a large rapidity gap from a low mass proton remnant system Y. The cross section is given in the deep-inelastic kinematic region of $2 < Q^2 < 100$ GeV^2 with inelasticity $0.05 < y < 0.7$. The diffractive kinematic region is defined by $x_{I\!P} < 0.04$, $M_Y < 1.6$ GeV and $|t| < 1$ GeV^2. The $D^{*\pm}$ mesons are restricted to the range $p_{T,D^*} > 2$ GeV and $|\eta_{D^*}| < 1.5$. The cross section is presented differentially as a function of various kinematic variables. The data are compared with NLO QCD calculations using the recent H1 diffractive PDF's as well as with a model of 2-gluon exchange.

1 Introduction

This paper presents a measurement of diffractive $D^{*\pm}$ production in deep inelastic scattering at HERA. This process is illustrated in Fig. 1. It is characterized by two distinct hadronic systems X and Y which are separated by a large rapidity gap. The system X contains at least one $D^{*\pm}$ meson, whereas Y consists of the elastically scattered proton or a low mass diffractive state. As a hard scale is already provided by the charm quark mass, diffractive charm production is interesting to test different perturbative QCD approaches to diffraction.

There are essentially two different ways theoretically to describe hard diffractive processes: the collinear factorization approach using diffractive parton densities [1], defined in analogy to the inclusive parton densities of the proton, and the k_t-factorization approach with 2-gluon exchanges using un-integrated gluon densities [2]. Whereas the former approach makes no a priori statement about the nature of the diffractive mechanism, the latter describes diffraction as the exchange of a colorless two (or more) gluon state.

In the collinear factorization approach diffractive parton densities are applied, which are obtained from next-to-leading order (NLO) QCD fits to the reduced diffractive cross section [3]. Charm production proceeds dominantly via the Boson Gluon Fusion process (BGF), as depicted in Fig. 1. According to the factorization theorem [1], the hard scattering matrix elements are the same as for inclusive heavy flavor production. Thus diffractive charm production is directely sensitive to the diffractive gluon density, which is only indirectly constrained in inclusive measurements of diffraction via scaling violations. For color compensation the system X (see Fig. 1) contains a diffractive remnant in addition to the $c\bar{c}$ pair.

In the perturbative 2-gluon approach, the non-diffractive un-integrated gluon densities in the proton are combined to a colorless 2-gluon state. This state can couple directly to the $c\bar{c}$ pair ($\gamma^* p \to c\bar{c}\ p$) or to a $c\bar{c}g$ system ($\gamma^* p \to c\bar{c}g\ p$). In the latter case, the gluon may have significant transverse momentum, in contrast to the remnant in the collinear factorisation approach.

In this paper the diffractive production of $D^{*\pm}$ mesons is investigated in the deep inelastic scattering regime, where the large photon virtuality provides a further hard scale in addition to the charm quark mass. The measurement is performed with the H1 detector at HERA and is based on a three times larger sample than in a previous publication [4], allowing for more differential investigations. The results are compared with predictions using both the collinear factorisation and the 2-gluon exchange approaches.

The paper is organized as follows: The kinematics of diffractive DIS are introduced in section 2. In section 3, the H1 detector and the data selection, are described. The cross section measurement and the evaluation of the systematic uncertainties are explained in section 4. In section 5 the results are presented and discussed.

2 Kinematics

The process studied in this paper is shown in Fig. 1. The electron couples to a virtual photon $\gamma^\star$ (with four-momentum q) which interacts with the proton (with four-momentum P). The

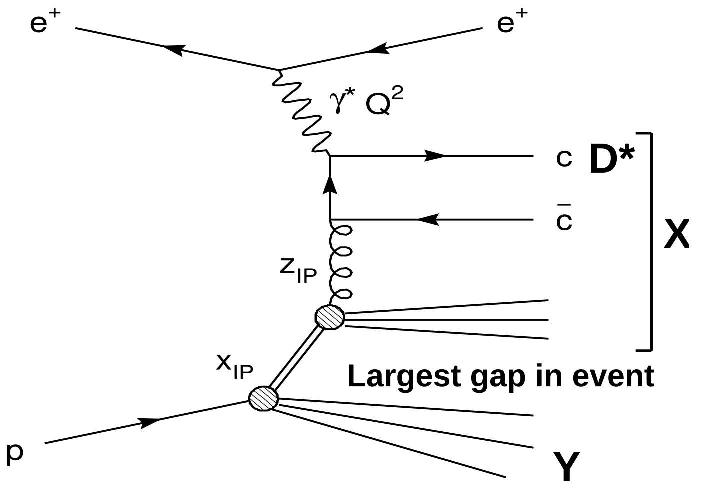

Figure 1: *The process under study in this article is $ep \to eXY \to e(D^{*\pm}X')Y$. The electron ($e$) couples to a photon ($\gamma^\star$) which interacts with the proton (p) via a color singlet exchange, producing two distinct final state hadronic systems X and Y. The systems X and Y are separated by the largest gap in rapidity between the final state hadrons.*

photon and the proton dissociate into two distinct hadronic systems X and Y, with invariant masses M_X and M_Y, respectively. The two systems are separated by a large rapidity gap. In addition to the standard DIS kinematic variables Q^2, y and Bjorken x the following variables are defined

$$x_{I\!P} = \frac{q \cdot (P - p_Y)}{q \cdot P}\,; \qquad t = (P - p_Y)^2\,; \qquad \beta = \frac{Q^2}{2q \cdot (P - p_Y)} = \frac{x}{x_{I\!P}}; \tag{1}$$

where p_Y is the four-momentum of Y. The quantity $x_{I\!P}$ may be interpreted as the longitudinal momentum fraction of the colorless exchange, with respect to the incoming proton. The variable t is the squared four-momentum transferred at the proton vertex. The variable β can be interpreted as the fractional longitudinal momentum of the colorless exchange carried by the struck quark. In this analysis t and M_Y are constrained to be small by the experimental selection and are integrated over implicitly. Furthermore the variable $z_{I\!P}$ is introduced as

$$z_{I\!P} = \beta \cdot \left(1 + \frac{\hat{s}}{Q^2}\right) = \frac{Q^2 + \hat{s}}{Q^2 + M_X^2}, \tag{2}$$

where $\hat{s}$ denotes the invariant mass of the charm quark pair emerging from the hard subprocess. $z_{I\!P}$ is an estimator for the fraction of the colour singlet exchange momentum, which enters the hard scattering.

3 Experimental aspects and data analysis

The data used for this analysis were taken in the years 1999 and 2000, when HERA collided positrons of energy $E_e = 27.5$ GeV with protons of energy $E_p = 920$ GeV. Requiring all detectors which are essential for this analysis to be fully operational results in an integrated luminosity of 42.6 pb^{-1}.

3.1 The H1 Detector

The H1 detector is described in detail in [5]. Only the components most relevant for this analysis are briefly discussed in this section. The coordinate system used has its origin at the nominal e^+p interaction point. Its z-axis in the outgoing proton direction is referred to as the 'forward' direction. Charged particles emerging from the interaction region are measured by the central tracking detector (CTD) in the range of $-1.5 < \eta < 1.5$[1]. The CTD comprises two large cylindrical central jet drift chambers (CJC) and two z chambers situated concentrically around the beam-line within a solenoidal magnetic field of 1.15 T. The CTD also provides triggering information based on track segments in the $r - \phi$ plane from the CJC and the position of the vertex using a double layer of multi-wire proportional chambers (MWPC). The energies of final state particles are measured in the Liquid Argon (LAr) calorimeter, which surrounds the tracking chambers and covers the range of $-1.5 < \eta < 3.4$. The backward region ($-4.0 < \eta < -1.4$) is covered by a lead-scintillating fiber calorimeter (SPACAL [6]) with electromagnetic and hadronic sections.

In the direction of the outgoing protons several detectors are installed close to the beam pipe which are used in the selection of large rapidity gap events. The Forward Muon Detector (FMD) is located at $z = 6.5$ m. It can detect particles directly in the region $1.9 < \eta < 3.7$, and from larger pseudorapidities via beam-pipe scattering. The PLUG calorimeter measures energies in the range of $3.5 < \eta < 5.5$. The Proton Remnant Tagger (PRT) consists of scintillators surrounding the beam pipe at $z = 26$ m. It tags hadrons in the region of $6.0 \lesssim \eta \lesssim 7.5$.

3.2 Event Selection

The selected events were triggered by an electromagnetic energy cluster in the SPACAL, in coincidence with a charged track signal recorded in both the MWPC and the CJC and a reconstructed event vertex. In the offline analysis the scattered positron is selected as an electromagnetic SPACAL cluster with energy $E'_e > 8$ GeV. The DIS kinematic variables Q^2 and y are reconstructed from the energy and polar angle of the scattered positron. The scaling variable Bjorken x is subsequently calculated from $x = Q/ys$ where s denotes the ep center-of-mass energy squared. The accepted kinematic range is $2 < Q^2 < 100\ \mathrm{GeV}^2$ and $0.05 < y < 0.7$.

Diffractive events are selected by demanding no detector activity above noise thresholds in the forward detectors, i.e. the PRT, the FMD, the PLUG and the most forward part ($\eta > 3.2$) of the LAr calorimeter. Using Monte Carlo simulations the data are then corrected to the range of the proton remnant system of $M_Y < 1.6$ GeV and the squared four-momentum transfer to the proton of $|t| < 1\ \mathrm{GeV}^2$. The four-momentum of the photon dissociation system X, which

[1] The pseudorapidity η of an object detected with polar angle θ is defined as $\eta = -\ln\ \tan(\theta/2)$.

is well contained in the central detector, is reconstructed using information from the LAr and SPACAL calorimeters and the CTD [7]. The variable $x_{I\!P}$ is calculated from

$$x_{I\!P} = \frac{Q^2 + M_X^2}{Q^2 + W^2}, \tag{3}$$

where W is the photon-proton center of mass energy which is given by $W^2 = ys - Q^2$. The kinematic range is restricted to $x_{I\!P} < 0.04$, which suppresses contributions from non-diffractive scattering and secondary reggeon exchanges. The quantity β is calculated from $\beta = x/x_{I\!P}$. The observable $z_{I\!P}^{obs}$ is defined as

$$z_{I\!P}^{obs} = \frac{M_{c\bar{c}}^2 + Q^2}{M_X^2 + Q^2}, \tag{4}$$

where $M_{c\bar{c}}^2$ is a hadron level estimate of $\hat{s}$ which is reconstructed from the scattered positron and the $D^{*\pm}$ meson. Further details are given in [4].

3.3 D^* identification

The D^{*+} mesons are reconstructed using the decay channel

$$D^{*+} \rightarrow D^0 \pi^+_{slow} \rightarrow (K^- \pi^+) \pi^+_{slow} \ \ (+c.c.), \tag{5}$$

which has a branching fraction of 2.57% [8]. The decay products are detected in the CTD. To ensure good detection efficiency and to reduce combinatorial background, the tracks are required to lie within the angular range of $20^{\mathrm{o}} < \theta < 160^{\mathrm{o}}$ and to have a transverse momentum p_T relative to the beam axis of at least 120 MeV for the π_{slow}, 300 MeV for the other π and 500 MeV for the K. The invariant mass of the $K\pi$ combination has to be consistent with the D^0 mass within ± 80 MeV. Furthermore the direction of the reconstructed $D^{*\pm}$ candidate is restricted to $|\eta(D^{*\pm})| < 1.5$ and its transverse momentum to $p_T(D^{*\pm}) > 2$ GeV. In Fig. 2 the distribution of the mass difference $\Delta M = M(K^{\mp}\pi^{\pm}\pi^{\pm}_{slow}) - M(K^{\mp}\pi^{\pm})$ is shown for all selected events and all track combinations which fulfill the above requirements. The number of $D^{*\pm}$ mesons is determined by fitting the ΔM spectrum with a Gaussian distribution for the signal together with a background parameterized as $a(\Delta M - m_\pi)^b(1 - c\,(\Delta M)^2)$, where m_π is the mass of the charged pion. The resulting number of identified $D^{*\pm}$ mesons is 140 ± 16.

4 Cross Section determination and systematic errors

The differential cross sections are obtained from fits to the ΔM distributions performed separately in each kinematic bin. The fits yield numbers of detected $D^{*\pm}$ mesons, which are translated into $D^{*\pm}$ cross sections by dividing by the branching ratio of the selected $D^{*\pm}$ decay channel and the integrated luminosity. Further corrections are applied for detector efficiencies, acceptances and migrations due to the finite resolution of the H1 detector. These corrections are calculated by running the H1 detector simulation program on a sample of $D^{*\pm}$ events produced by the diffractive Monte Carlo generator RAPGAP [9, 10] using diffractive parton densities. The RAPGAP program is used to model events which contain an elastically scattered proton

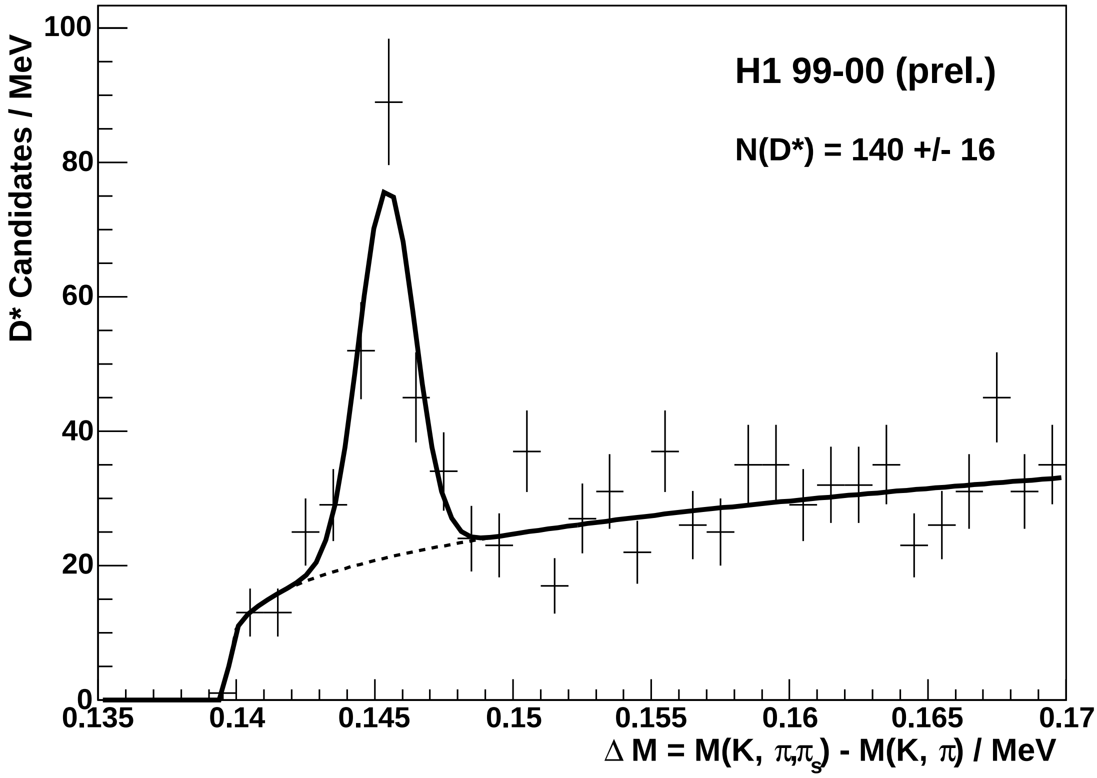

Figure 2: *Distribution of the mass difference* $\Delta M = M(K^{\mp}\pi^{\pm}\pi^{\pm}_{slow}) - M(K^{\mp}\pi^{\pm})$. *The fitted curve is of the form* $a(\Delta M - m_{\pi})^{b}(1 - c\,(\Delta M)^{2}) +$ *Gaussian function for the signal.*

($M_Y = m_p$) in the kinematic range $x_{I\!P} < 0.1$. Migrations from $x_{I\!P} > 0.1$ or from large values of M_Y ($M_Y > 5$ GeV) are modeled by using the RAPGAP program in its non-diffractive mode. This contribution is of the order of 1% of the selected sample of events. An additional correction of 10% is applied to account for the net smearing across the $M_Y = 1.6$ GeV boundary. Since only elastically scattered protons are simulated in RAPGAP , this correction is evaluated using the proton dissociation simulation in the DIFFVM [11, 12] generator[2].

The following sources of systematic uncertainties and the resulting influence on the cross section measurement have been studied:

- The uncertainty on the trigger efficiency is taken from a comparison of the efficiency determined from data using a monitor trigger sample and the result of a Monte Carlo simulation and is estimated to be $\pm 3\%$.
- Varying the reconstructed energy and polar angle of the scattered electron within the estimated uncertainties on the resolution and energy scale of the SPACAL results in an uncertainty of $\pm 3\%$.

[2]For the correction, it is assumed that the ratio of diffractive proton elastic to diffractive proton dissociative interactions is 1 : 1.

- The track reconstruction efficiency and uncertainties related to the signal extraction from the fit to the ΔM distribution have been determined by analyzing an inclusive D^* sample and are estimated to be $^{+11\%}_{-6\%}$ and $\pm 3\%$, respectively.

- The uncertainty in the hadronic energy scale of the liquid argon calorimeter is taken into account by varying (in the Monte Carlo simulation) the energies of the reconstructed hadronic final state by 4%. This affects the M_X reconstruction and leads to changes of the cross section of $\pm 4\%$.

- As an estimate of the uncertainty in the acceptance and migration corrections due to uncertainties in the physics model for diffractive $D^{*\pm}$ production, the effect of varying in the simulation the shape of various kinematic distributions within limits set by previous measurements have been studied. Reweighting the $x_{I\!P}$ distribution on the generator level by $(1/x_{I\!P})^{\pm 0.05}$, the β distribution by $(1 \pm 1.5\beta)$, the M_Y distribution by $(1/M_Y)^{\pm 0.3}$, the $|t|$ distribution for elastic scattering by $e^{\pm 2|t|}$, the $|t|$ distribution for proton dissociation by $e^{\pm |t|}$ and varying the assumed ratio of proton-dissociative to proton-elastic cross sections from $1:2$ to $2:1$, results in a systematic uncertainty of $\pm 12\%$ on the cross section.

- As an estimate of the uncertainty in the charm fragmentation scheme the default parameterization of the Peterson model was changed to the Lund string model [13] in the simulation, leading to a change in the measured cross section of -3%.

The total systematic error for each data point has been obtained by adding all individual contributions in quadrature. It ranges between 15% and 28%.

5 Results

The visible cross section for the kinematic region $2 < Q^2 < 100$ GeV^2, $0.05 < y < 0.7$, $x_{I\!P} < 0.04$, $M_Y < 1.6$ GeV, $|t| < 1$ GeV^2, $p_{T,D^*} > 2$ GeV and $|\eta_{D^*}| < 1.5$ is measured to be

$$\sigma(ep \to (D^{*\pm}X')Y) = 333 \pm 38(stat.) \pm 57(syst.) \text{ pb.} \tag{6}$$

This is in agreement with the value of $246 \pm 54(stat.) \pm 56(syst.)$ pb which was found for the same kinematic range in the previous H1 measurement [4]. It is also interesting to compare the measurement to the published measurement of the ZEUS collaboration [14], which is quoted in a slightly different phase space, which mainly originates from a lower cut in $p_T(D^{*\pm})$. Using the RAPGAP Monte Carlo generator [9, 10] to rescale the ZEUS measurement to the kinematic range of this paper (correction factor of $C = 0.58$ with an additional 10 % correction for the different M_Y ranges), results in a cross section value of $305 \pm 25(stat.)^{+20}_{-34}(syst.)$ pb, which is in good agreement with the measurement quoted above.

The cross section for the kinematic region, as defined above, but for $x_{I\!P} < 0.01$ is measured to be

$$\sigma(ep \to (D^{*\pm}X')Y) = 131 \pm 24(stat.) \pm 24(syst.) \text{ pb.} \tag{7}$$

$x_{I\!P} < 0.04$		cross section
H1 Data		333 ± 38 (stat.) ± 54 (syst.) pb
collinear factorization - diffractive pdfs		
H1 2002 prel [3]	NLO [15, 16]	$241 \pm^{66}_{39}$ pb
H1 2002 prel [3]	ME+PS [9, 10]	224 pb
$x_{I\!P} < 0.01$		
H1 Data		131 ± 24 (stat.) ± 24 (syst.) pb
collinear factorization - diffractive pdfs		
H1 2002 prel [3]	NLO [15, 16]	$76 \pm^{17}_{10}$ pb
H1 2002 prel [3]	ME+PS [9, 10]	76 pb
k_t - factorization - two gluon		
CCFM set 1 [17]	BJKLW [2, 18, 19] ($p_T > 1.5$ GeV)	139 pb

Table 1: *Predictions of different calculations for the total diffractive $D^{*\pm}$ cross section in the kinematic regions $x_{I\!P} < 0.04$ and $x_{I\!P} < 0.01$ compared with the measured cross sections.*

5.1 Comparisons with calculations

In Tabel 1 the total visible cross section is compared with predictions from different theoretical models. For all calculations the charm mass was set to $m_c = 1.5$ GeV, Λ_{QCD} was chosen to be to 0.20 GeV and the number of active quark flavors in the expression for α_s was taken to be $N_f = 4$. The data are compared with two calculations based on the collinear factorization approach, using the parton distributions obtained from the LO (NLO) DGLAP analysis of the reduced diffractive cross section from H1 [3]:

- A next-to-leading order (NLO) calculation using a diffractive version of the program HVQDIS [15, 16] with the NLO diffractive parton densities. For this calculation the renormalization and factorisation scales were set to $\mu_f^2 = \mu_r^2 = Q^2 + 4m_c^2$. The Peterson fragmentation function was used with $\epsilon = 0.078$. The uncertainties on the NLO calculation correspond to a variation of the renormalization scale (preserving $\mu_f = \mu_r$) by factors of $1/4$ and 4, a variation of the charm mass within $m_c = 1.35...1.65$ GeV and a variation of the ϵ parameter between 0.035 and 0.1. These variations are performed separately and the uncertainties are added in quadrature.

- A calculation based on $\mathcal{O}(\alpha_s)$ matrix elements and the LO diffractive parton densities, supplemented with initial and final state parton showers as implemented in the Monte Carlo event generator RAPGAP [9, 10]. The D^* meson was fragmented according to the Lund string model [13]. The renormalization scale and the factorization scale were set to $\mu_f^2 = \mu_r^2 = Q^2 + p_T^2 + 4m_c^2$. The LO version of the diffractive parton densities were used [3]. For the numbers presented here, no variation of scales, the charm-quark mass or the fragmentation parameters was performed.

The calculated cross sections for the two models are given in Tab. 1 and are found to be lower than the data in both regions $x_{I\!P} < 0.04$ and $x_{I\!P} < 0.01$. However, the predictions are still consistent with the data within the estimated experimental and theoretical uncertainties. The agreement between data and the NLO calculation supports the validity of the hard scattering factorization which is applied in the calculations.

For $x_{I\!P} < 0.01$ the data are also compared to a prediction from the perturbative 2-gluon approach 'BJKLW' [2, 18, 19] using the un-integrated gluon density [17] obtained from the inclusive structure function F_2 evolved by the CCFM evolution equations. These calculations in the perturbative 2-gluon approach are applicable only in the region of small $x_{I\!P}$, where contributions from quark exchange can be neglected. As this calculation is valid only in the perturbative region, a cut on the transverse momentum of the gluon needs to be applied for the process $c\bar{c}g$, which is also shown in Tab. 1. Using a cut of $p_T > 1.5\,\mathrm{GeV}$ the visible cross section in the range $x_{I\!P} < 0.01$ is well reproduced. Varying the cut to $p_T > 2\,\mathrm{GeV}$ leads to a $\sim 7\%$ variation of the cross section.

5.2 Differential cross sections

Measurements for $\boldsymbol{x_{I\!P} < 0.04}$: In Figs. 3 and 4 cross sections differential in various variables are shown and compared to the NLO calculation [15, 16] in the collinear approach (for details see previous section). The cross sections represent average values over the intervals shown in the figures. In Fig. 3 the cross section is shown as a function of the variables $x_{I\!P}$, β and $z_{I\!P}^{obs}$. Figure 4 shows the cross section as a function of the event kinematic variables Q^2 and y and as a function of the $D^{*\pm}$ transverse momentum p_T and rapidity η. As can be seen from Figs. 3 and 4, the differential cross sections are reproduced by the NLO calculation within the uncertainties in all quantities shown. In Fig. 5 the cross section in $x_{I\!P}$ is shown again together with the predictions from the NLO calculation and from the LO calculation as implemented in RAPGAP [9, 10] (for details see previous section). As can be seen from Fig. 5 the predictions from RAPGAP are in agreement with the full NLO calculations. In Fig. 6 the cross section is shown as a function of p_T and compared to the measurement of ZEUS [14]. The ZEUS data points were rescaled to the kinematic range of this paper, using the RAPGAP Monte Carlo generator [9, 10] and applying an additional 10 % correction for the different M_Y range. Both measurements are in good agreement.

Measurements for $\boldsymbol{x_{I\!P} < 0.01}$: In Fig. 7 the differential cross sections for the region $x_{I\!P} < 0.01$ are shown and compared both to the NLO calculation [15, 16] and to the prediction from the perturbative 2-gluon calculation of *BJKLW* [2, 18, 19]. The NLO calculation falls below the data in all differential bins, but still agrees within errors. The perturbative 2-gluon calculation of *BJKLW* uses an un-integrated gluon density, which is taken from inclusive measurements [17]. No extra free parameter or assumption for the diffractive mechanism is introduced except for the choice of the cut-off at $p_T > 1.5\,\mathrm{GeV}$ for the gluon in the $c\bar{c}g$ process. With this cut-off inclusive jet data are described well [20]. As can be seen in Fig. 7 also the diffractive $D^{*\pm}$ measurement is described well in all differential bins.

6 Conclusion

A new measurement of diffractive open charm production in DIS at HERA has been presented using an integrated luminosity of 42.6 pb^{-1} corresponding to a data sample three times larger than in a previous publication [4]. The total $D^{*\pm}$ production cross section in the kinematic range of $2 < Q^2 < 100\ \mathrm{GeV}^2$, $0.05 < y < 0.7$, $x_{I\!P} < 0.04$, $M_Y < 1.6\ \mathrm{GeV}$, $|t| < 1\ \mathrm{GeV}^2$, $p_{T,D^*} > 2\ \mathrm{GeV}$ and $|\eta_{D^*}| < 1.5$ is measured to be $333 \pm 38\ (\mathrm{stat.}) \pm 54\ (\mathrm{syst.})\ \mathrm{pb}$. This measurement is in agreement with previous measurements of H1 [4] and ZEUS [14]. When restricting the measurement to the range $x_{I\!P} < 0.01$ the cross section reduces to $131 \pm 24(stat.) \pm 24(syst.)\ \mathrm{pb}$. The cross section has been measured differentially as a function of various kinematic variables. Different QCD calculations are compared with the measurement. Calculations based on H1 diffractive parton densities, extracted from fits to $F_2^{D(3)}$ in the collinear factorization approach and performed in leading and next-to-leading order pQCD, are below the data but still agree within the errors. They describe the observed shapes of the differential cross sections well. The agreement supports the validity of the hard scattering factorization, whereby diffractive parton densities determined from inclusive diffractive processes are universal and can be applied to predict exclusive processes such as charm production or diffractive dijet production [21–23], which probe the gluonic content of the parton densities. In the restricted kinematic region of $x_{I\!P} < 0.01$ the data are also compared to the predictions of a calculation based on the perturbative 2-gluon approach using an un-integrated gluon density, with which good agreement of the calculation is observed in both the measured inclusive cross section and in all differential cross sections.

References

[1] J. Collins, *Phys. Rev.* **D 57** (1998) 3051, ERRATUM-ibid. **D 61** (2000), hep-ph/9709499.

[2] J. Bartels, H. Jung, A. Kyrieleis, *Eur. Phys. J.* **C 24** (2002) 555, hep-ph/0204269.

[3] H1 Collaboration;, *Measurement and NLO DGLAP QCD Interpretation of Diffractive Deep-Inelastic Scattering at HERA*, paper 980 submitted to 31st ICHEP02, Amsterdam (2002), https://www-h1.desy.de/h1/www/publications/htmlsplit/H1prelim-03-011.long.html.

[4] H1 Collaboration; C. Adloff et al., *Phys. Lett.* **B 520** (2001) 191, hep-ex/0108047.

[5] H1 Collaboration; I. Abt et al., *Nucl. Instrum. Meth.* **A386** (1997) 310,348.

[6] H1 Collaboration; R. D. Appuhn et al, *Nucl. Instrum. Meth.* **A386** (1997) 397.

[7] H1 Collaboration; C. Adloff et al., *Z. Phys.* **C74** (1997) 221.

[8] S. Eidelman et al., *Phys. Lett.* **B592** (2004) 1.

[9] H. Jung, *Comp. Phys. Comm.* **86** (1995) 147.

[10] H. Jung, *The RAPGAP Monte Carlo for Deep Inelastic Scattering, version 2.08*, Lund University, 2002, `http://www-h1.desy.de/~jung/rapgap/`.

[11] B. List, Diploma thesis, Techn. Univ. Berlin (unpublished).

[12] B. List, A. Mastroberardino, *DIFFVM: A Monte Carlo generator for diffractive processes in e p scattering*, in *Proceedings of the Workshop on Monte Carlo generators for HERA physics*, edited by A. Doyle, G. Grindhammer, G. Ingelman, H. Jung (DESY, Hamburg, 1999), p. 396.

[13] T. Sjöstrand, *Comp. Phys. Comm.* **82** (1994) 74.

[14] ZEUS Collaboration; S. Chekanov et al, *Nucl. Phys.* **B672** (2003) 3, hep-ex/0307068.

[15] B. W. Harris, J. Smith, *Nucl. Phys.* **B452** (1995) 109, hep-ph/9503484.

[16] L. Alvero, J. C. Collins, J. J. Whitmore, *PSU-TH-* **200** (1998) 13, hep-ph/9806340.

[17] M. Hansson, H. Jung, *The status of CCFM unintegrated gluon densities*, DIS 2003, St. Petersburg, Russia, hep-ph/0309009.

[18] J. Bartels, H. Lotter, M. Wüsthoff, *Phys. Lett.* **B 379** (1996) 239, ERRATUM-ibid. **B 382** (1996) 449, hep-ph/9602363.

[19] J. Bartels, H. Jung, M. Wusthoff, *Eur. Phys. J.* **C 11** (1999) 111, hep-ph/9903265.

[20] A. Aktas et al., *Eur. Phys. J.* **C33** (2004) 477.

[21] H1 Collaboration; C. Adloff et al., *Eur. Phys. J.* **C 20** (2001) 29, hep-ex/0012051.

[22] H1 Collaboration;, *Comparison at NLO between Predictions from QCD Fits to F2D and Diffractive Final State Observables at HERA*, intl. Europhysics Conference on High Energy Physics, EPS03,Aachen (2003) Abstract:113 Session:5, https://www-h1.desy.de/h1/www/publications/htmlsplit/H1prelim-03-015.long.html.

[23] H1 Collaboration;, *Comparison between diffractive dijet electroproduction and photoproduction*, submitted paper to ICHEP04,Beijing (2004) Abstract:177 Session:6.

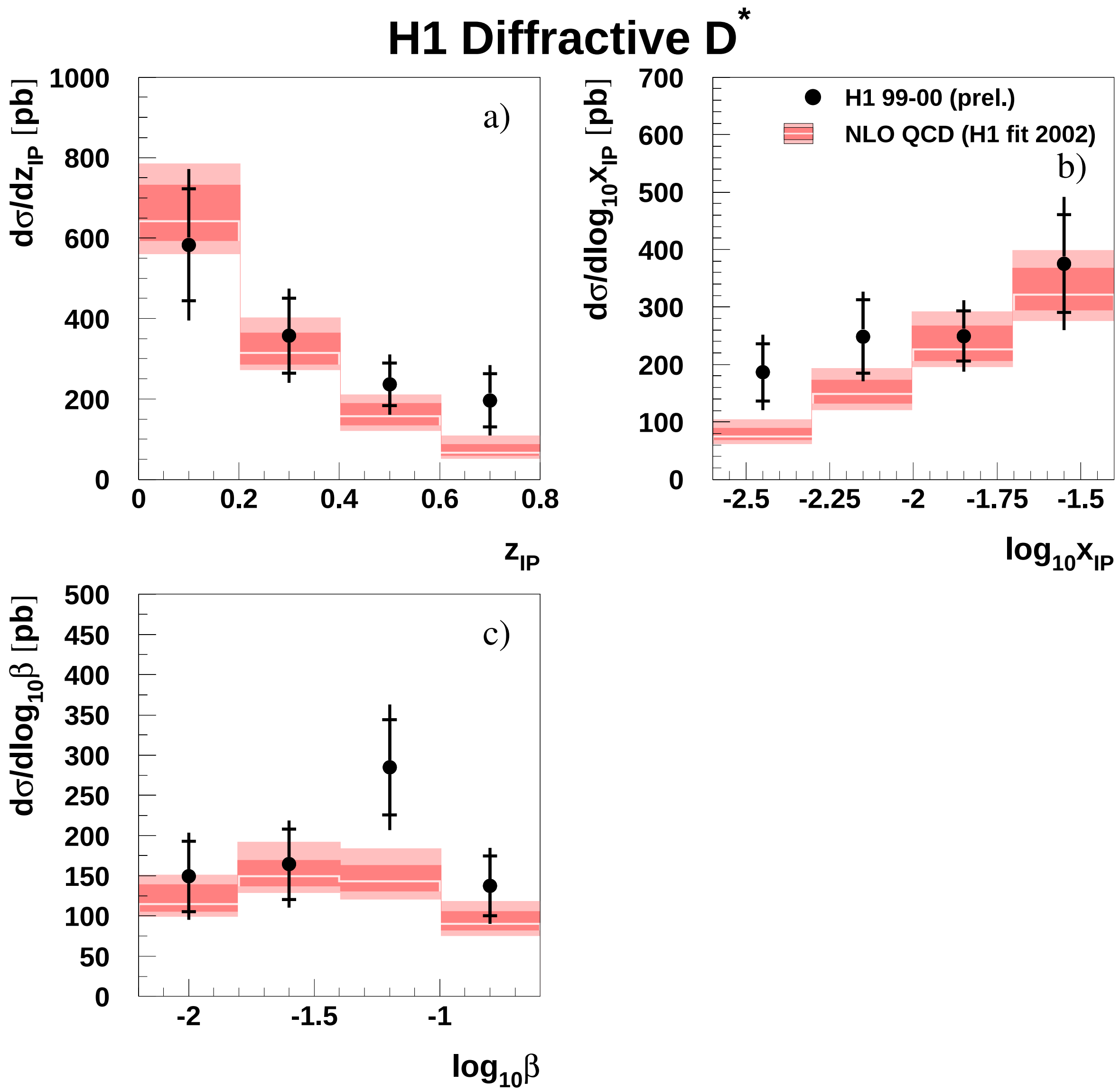

Figure 3: *Differential cross sections for D^* meson production in diffractive DIS, shown as a function of a) $z_{I\!P}$, an estimator for the longitudinal momentum fraction of the diffractive exchange entering the hard process, b) $x_{I\!P}$, the longitudinal proton momentum fraction taken by the diffractive exchange and c) β, an estimator for the longitudinal momentum fraction of the diffractive exchange carried by the struck quark. All cross sections represent the average value over the corresponding bin. The data are shown as points with error bars (inner: statistical, outer: total). They are compared with a next-to-leading order QCD calculation as implemented in a diffractive version of the program HVQDIS [15, 16], using the NLO diffractive parton distributions from [3]. The nominal predictions are shown as the central lines of the error bands. The inner error band represents the renormalization scale uncertainty, while the outer error band shows the total uncertainty, which includes variations of the charm mass in the range* $m_c = 1.35 \ldots 1.65$ GeV *and of the parameter of the Peterson fragmentation function* $\epsilon = 0.035 \ldots 0.100$, *added in quadrature.*

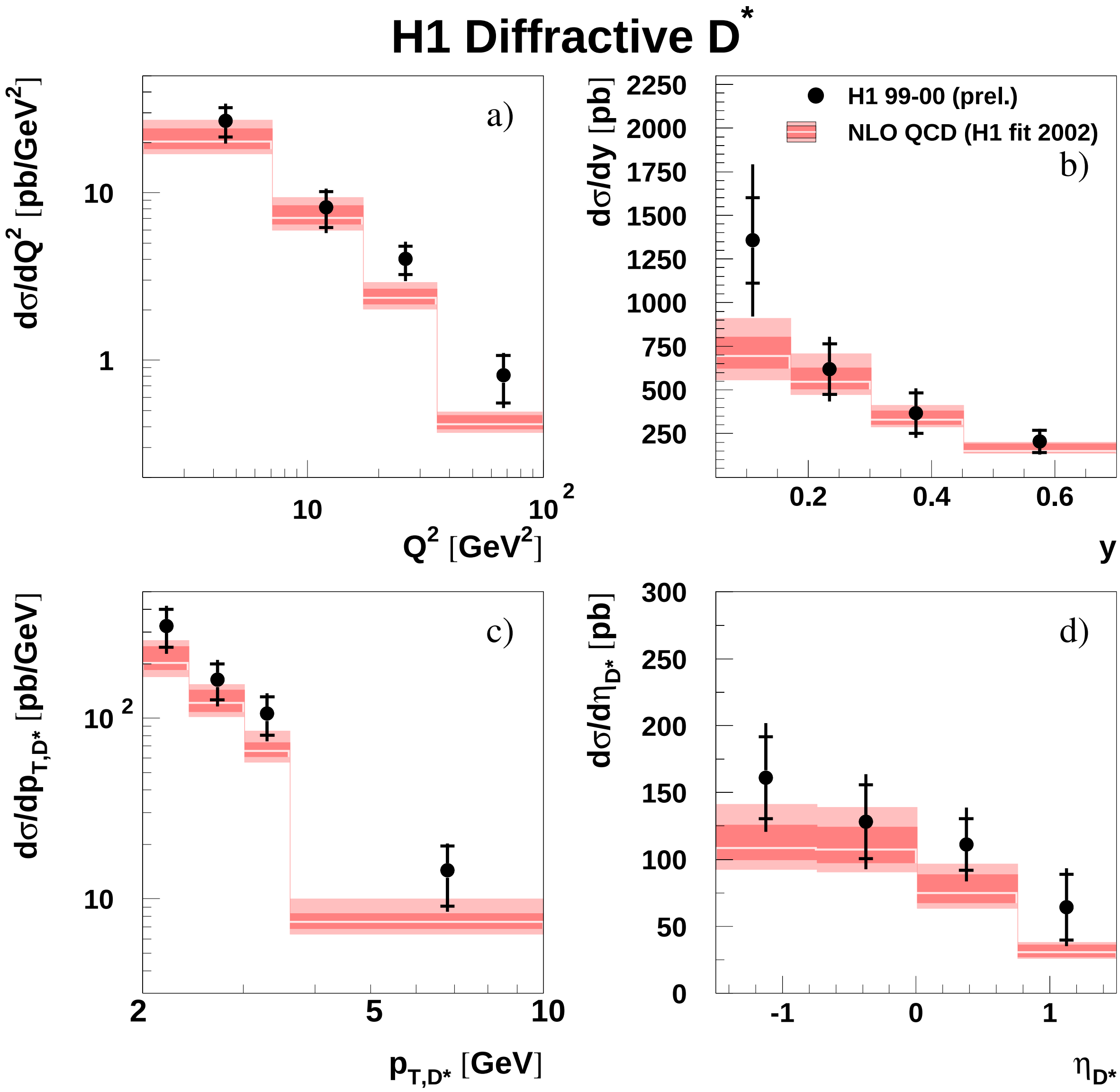

Figure 4: *Differential cross sections for D^* meson production in diffractive DIS, shown as a function of a) the photon virtuality Q^2, b) the inelasticity y, c) the transverse momentum p_{T,D^*} and d) the pseudorapitdy η_{D^*} of the $D^{*\pm}$ meson. All cross sections represent the average value over the corresponding bin. The data are shown as points with error bars (inner: statistical, outer: total). They are compared with a next-to-leading order QCD calculation [15, 16], using the NLO diffractive parton distributions from [3]. The nominal predictions are shown as the central lines of the error bands. For details see Fig. 3.*

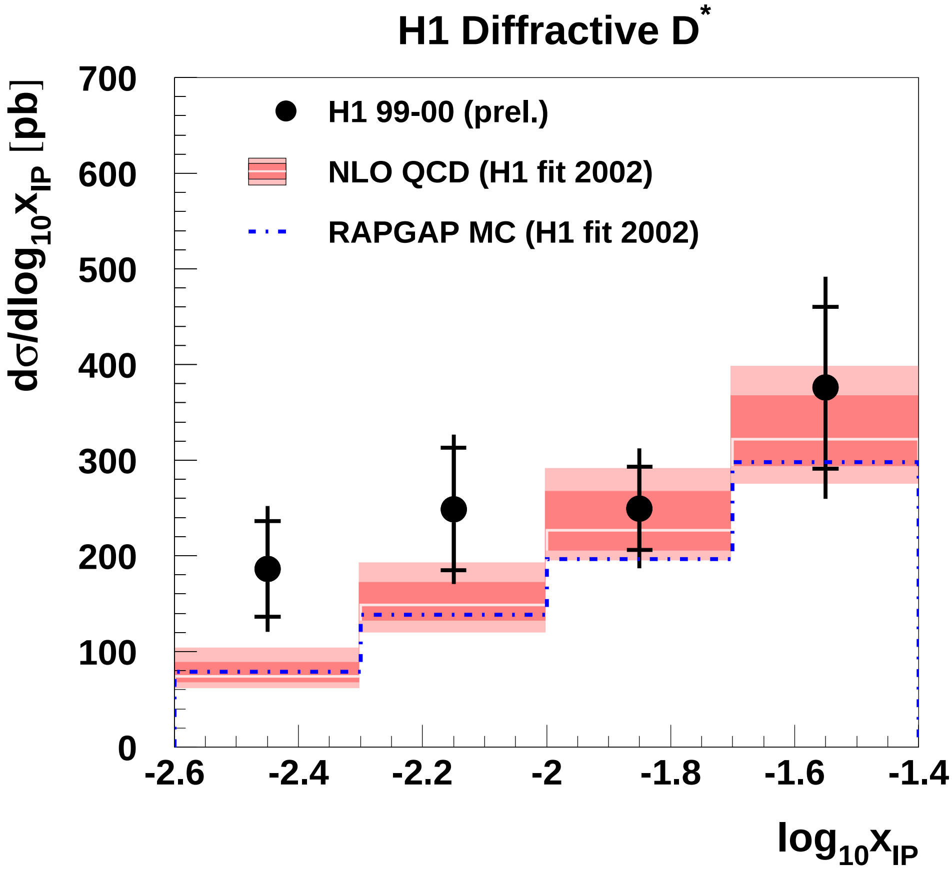

Figure 5: *Differential cross sections for D^* meson production in diffractive DIS, shown as a function of $x_{I\!P}$, the longitudinal proton momentum fraction taken by the diffractive exchange. All cross sections represent the average value over the corresponding bin. The data are shown as points with error bars (inner: statistical, outer: total). They are compared with a next-to-leading order QCD calculation [15,16], using the NLO diffractive parton distributions from [3]. For details see Fig. 3. Also shown are predictions obtained with the LO hadron level Monte Carlo event generator* RAPGAP *(dot-dashed curve).*

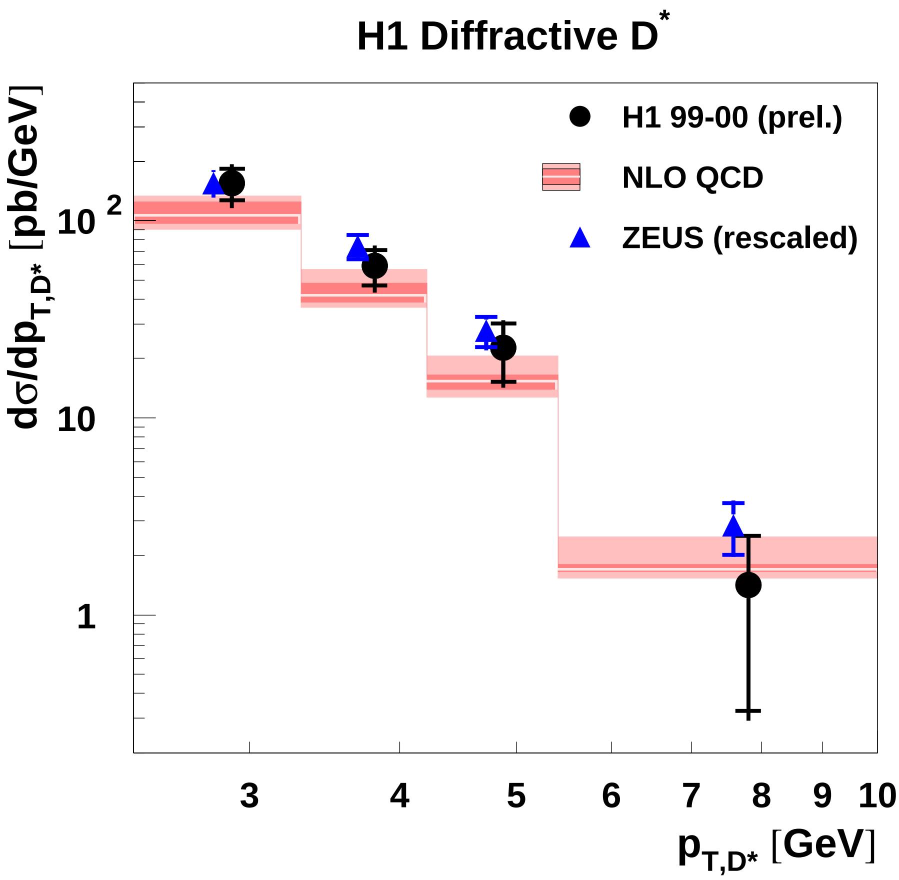

Figure 6: *Differential cross section for D^* meson production in diffractive DIS, shown as a function of the transverse momentum p_{T,D^*}. All cross sections represent the average value over the corresponding bin. The data are shown as points with error bars (inner: statistical, outer: total). They are compared with a next-to-leading order QCD calculation [15,16], using the NLO diffractive parton distributions from [3]. For details see Fig. 3. Also shown is the measurement from ZEUS [14], rescaled to the phase space region investigated here. For this comparison the binning has been changed. The data points of the ZEUS measurement are slightly displaced for visibility.*

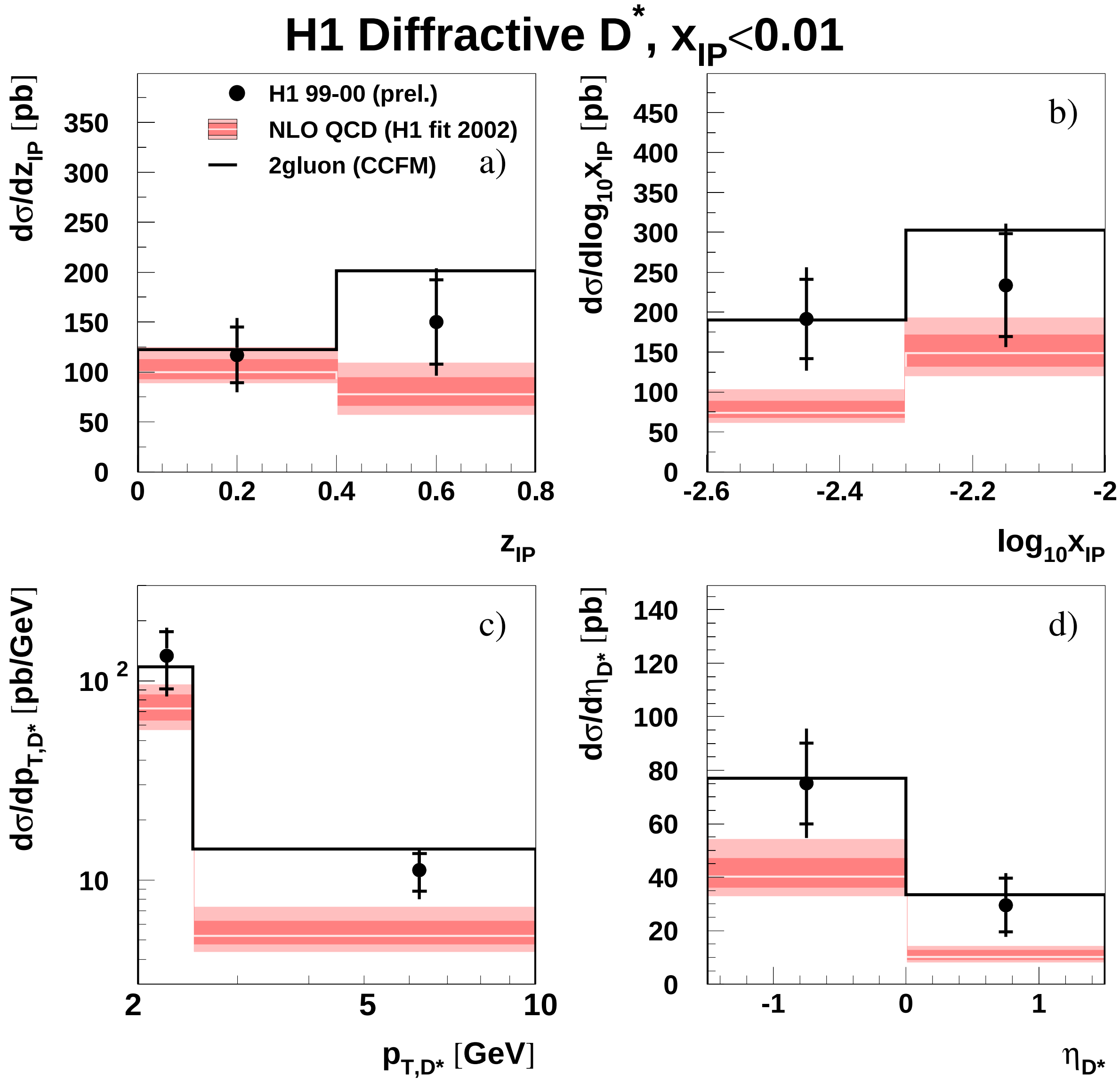

Figure 7: *Differential cross sections for D^* meson production in diffractive DIS, in the restricted kinematic region $x_{I\!P} < 0.01$, shown as a function of a) $z_{I\!P}$, an estimator for the longitudinal momentum fraction of the diffractive exchange entering the hard process, b) $x_{I\!P}$, the longitudinal proton momentum fraction taken by the diffractive exchange, c) the transverse momentum p_{T,D^*} and d) the pseudorapitdy η_{D^*} of the $D^{*\pm}$ meson. All cross sections represent the average value over the corresponding bin. The data are shown as points with error bars (inner: statistical, outer: total). They are compared with a next-to-leading order QCD calculation [15, 16], using the NLO diffractive parton distributions from [3]. The nominal predictions are shown as the central lines of the error bands. For details see Fig. 3. Also shown is a prediction from the perturbative 2-gluon approach of BJKLW [2, 18, 19] using the un-integrated gluon density obtained from a fit assuming CCFM evolution to the inclusive structure function F_2 [17] with a cut of $p_T > 1.5\,\mathrm{GeV}$ for the gluon in the $c\bar{c}g$ process (dot-dashed curve).*